Weak ferromagnetism and short range polar order in $NaMnF_3$ thin films

Amit KC,[1,2] Pavel Borisov,[1] Vladimir V. Shvartsman,[3] and David Lederman[1,2]
[1)]*Department of Physics, West Virginia University, Morgantown, WV 26506, USA*
[2)]*Department of Physics, University of California, Santa Cruz, CA 95064, USA*
[3)]*Institute for Materials Science, University of Duisburg-Essen, Universitätsstraße 15, 45141 Essen, Germany*

(Dated: 9 February 2017)

The orthorhombically distorted perovskite $NaMnF_3$ has been predicted to become ferroelectric if an $a = c$ distortion of the bulk *Pnma* structure is imposed. In order to test this prediction, $NaMnF_3$ thin films were grown on $SrTiO_3$ (001) single crystal substrates via molecular beam epitaxy. The best films were smooth and single phase with four different twin domains. In-plane magnetization measurements revealed the presence of antiferromagnetic ordering with weak ferromagnetism below the Néel temperature $T_N = 66$ K. For the dielectric studies, $NaMnF_3$ films were grown on a 30 nm $SrRuO_3$ (001) layer used as a bottom electrode grown via pulsed laser deposition. The complex permittivity as a function of frequency indicated a strong Debye-like relaxation contribution characterized by a distribution of relaxation times. A power-law divergence of the characteristic relaxation time revealed an order-disorder phase transition at 8 K. The slow relaxation dynamics indicated the formation of super-dipoles (superparaelectric moments) that extend over several unit cells, similar to polar nanoregions of relaxor ferroelectrics.

There is much interest in multiferroic (MF) materials that show coexistence of two or more long-range orders such as ferroelectricity, (anti-) ferromagnetism and/or ferroelasticity. Magnetoelectric (ME) coupling can allow for the control of magnetization $\mathbf{M}$ (electric polarization $\mathbf{P}$) using an electric field $\mathbf{E}$ (a magnetic field $\mathbf{H}$), which can be used for potential applications in data storage, sensors and spintronic devices.[1–5] As a result, there has been much effort expended towards synthesizing MF insulating materials with strong ME coupling at room temperature.[6–9]

Many MF materials are oxides, but multiferroicity can also be found in fluorides. For example, in the orthorhombic $BaMF_4$ family the $M =$ Co and Ni compounds in bulk form are ferroelectric (FE) and antiferromagnetic.[10] While in oxide perovskites ABO_3 the simultaneous presence of FE and magnetic orderings is limited by conflicting requirements for the d^n electronic configuration of the transition metal in the B-site,[11] ferroelectricity in $BaMnF_4$ is mainly due to geometric (topological) reasons.[12] Recent experiments showed that $BaCoF_4$ thin films are weakly ferromagnetic at low temperatures due to strain.[13]

$NaMnF_3$ (NMF) is another fluoride compound that is possibly MF with ME coupling. The NMF crystal structure is described by the orthorhombic space group *Pnma*. At room temperature, the lattice constants are $a_O = 5.751$ Å, $b_O = 8.008$ Å, and $c_O = 5.548$ Å (Fig. 1a).[14] In the pseudo-cubic unit cell, the corresponding lattice parameters are $a_{pc} = c_{pc} = \sqrt{a_O^2 + c_O^2}/2 = 3.995$ Å and $b_{pc} = b_O/2 = 4.004$ Å. NMF exhibits *G*-type antiferromagnetism of the Mn magnetic moments centered within tilted MnF_6 octahedra, with additional weak ferromagnetic canting.[14–16] The Néel temperature has been reported to be $T_N = 66$ K.[15–20] Recent computational work predicted a ferroelectric instability in NMF originating from Na displacements (the A-site perovskite cation in the ABF_3 structure). Calculations assuming that a cubic substrate forces the a and c lattice parameters to be equal to each other have shown that the soft polar mode B_{2u} freezes, resulting in a transformation to the polar $Pna2_1$ space group which causes a polarization of $P = 6$ μC/cm^2 along the long axis b. Calculations also indicate that P can be enhanced by negative or positive strains (12 μCcm^2 at $+5\%$ strain 9 μC/cm^2 at -5% strain).[21,22] A weak ferromagnetic phase and an amplification of ME coupling are also expected in the strained films, with a ME response comparable to Cr_2O_3.[22] Therefore, NMF is an attractive ME material because its ferroelectricity can be modulated by strain and is not subject to the d^n rule because there is no displacement of the Mn ion from the center of the MnF_6 octahedra.

Here we report on the growth of NMF thin films on cubic $SrTiO_3$ (STO) substrates and on $SrRuO_3$ (SRO) layers, their weak ferromagnetism (FM) below the T_N, and their short range dipolar order. NMF thin films approximately 50 nm thick were grown on pre-polished single crystal (001) STO substrates ($a = 3.905$ Å) by molecular beam epitaxy (MBE) by co-depositing NaF and MnF_2 in an ultra-high vacuum chamber with growth pressure $P \approx 5.0 \times 10^{-9}$ Torr. Atomically flat surface and single termination of STO substrates was achieved by the combination of two thermal annealing steps and a de-ionized (DI) water treatment.[23] For additional details of the growth process, see supplementary material. The crystallography of the substrate and film surfaces was monitored *in-situ* using reflection high energy electron diffraction (RHEED). Further crystallographic characterization was carried out *ex-situ* using x-ray diffraction (XRD) and x-ray reflectivity (XRR) techniques using a rotating anode source with a graphite bent crystal monochromator optimized for Cu K_α radiation. The surface morphology was studied by atomic force microscopy (AFM). Magnetic measurements were performed using a superconducting quantum interference device (SQUID) magnetometer with the substrate signal subtracted by performing identical measurements on a blank substrate.

Dielectric measurements of NMF films were performed by first depositing a 30 nm SRO film on the STO substrate as a bottom electrical contact via pulsed laser deposition (PLD) in a separate vacuum chamber. The SRO was grown at a substrate temperature of 600 °C in 100 mTorr O_2 partial pressure. A 150 nm NMF thin film was then deposited on the SRO us-

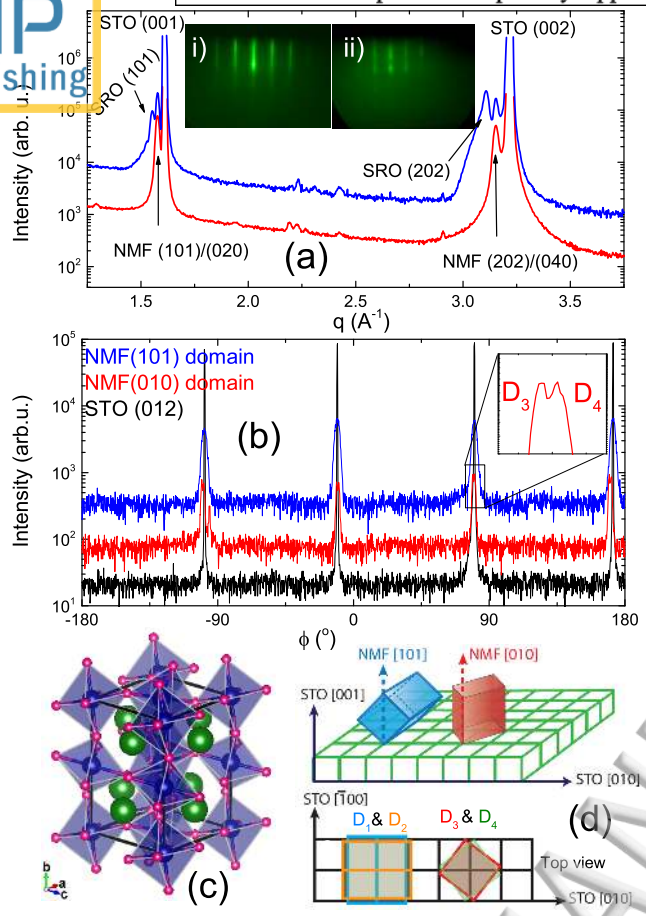

FIG. 1. (a) $\theta - 2\theta$ XRD scan of 50 nm NMF film on STO(001) and 150 nm NMF grown on 30 nm SRO on STO(001). Insets show RHEED patterns of the NMF/STO (i) and NMF/SRO (ii) films. (b) NMF/STO ϕ-scans corresponding to (012) reflections (black curve) of the substrate and $(222)_O$ reflections of the NMF(010) (red) and NMF(101) (blue) domains with χ (the angle between the scattering vector and surface normal) = 26.57°, 63.50°, and 26.50°, respectively. Inset shows a closeup of the NMF(010) domain indicating twinning of the $(222)_O$ planes. (c) NMF orthorhombic unit cell with MnF_6 octahedra. Green, blue and pink spheres are Na, Mn and F ions, respectively. (d) Schematic of the epitaxial orientation of NMF/STO with top views of NMF(101) and NMF(010) domains determined from ϕ-scans.

ing the conditions described above. The dielectric constant was measured using a lock-in amplifier in the frequency range of 100 Hz to 100 kHz from 10 K to room temperature using a cryostat and an ac voltage amplitude of $V_{ac} = 100$ mV. Similar results were obtained for $V_{ac} = 10$ mV.

The best film quality was achieved at T_s= 250 and 300 °C as determined from XRD and RHEED. Figure 1a shows the $\theta - 2\theta$ XRD scan for a film grown at $T_s = 300$ °C. The out-of-plane lattice parameters were 3.989 Å and 3.982 Å, and the rocking curve full width at half maximum (FWHM) values were 1.32° and 2.23° for NMF/STO and NMF/SRO films, respectively (see supplementary material). The positions of the SRO peaks were consistent with data in the literature.[24] XRR data (supplementary material) were fitted using GenX software for the NMF/STO film[25] to obtain a NMF thickness of 51.76 nm and a NMF surface surface roughness of 0.4 nm. Streaky RHEED patterns (Fig. 1a inset i) confirmed that the NMF/STO film was smooth and crystalline while the NMF/SRO sample also had streaky patterns with a somewhat fuzzy streaky background (Fig. 1a inset ii).

Using the *Pnma* NMF structure, reflections associated with b_O-axis pointing out-of-plane [NMF(010)/STO(001)] as well as in-plane [NMF(101)/STO(001)] domains were identified via XRD ϕ-scans and reciprocal space maps (RSMs) (the corresponding (010) and (101) lattice parameters are virtually identical; see supplementary material Fig. S4 for RSM data). These results indicate the absence of $a_O = c_O$ distortion in the NMF/STO film for both of these domains. The measured lattice parameters for NMF(010)/STO(001) and NMF(101)/STO(001) domains were $a_O = 5.76$ Å, $b_O = 7.98$ Å, and $c_O = 5.57$ Å and $a_O = 5.86$ Å, $b_O = 8.04$ Å, and $c_O = 5.45$ Å respectively (see Table S1 in the supplementary material). Figure 1b shows the ϕ-scans of the $(222)_O$ reflection of the NMF(101) and NMF(010) domains along with (012) reflections of the substrate. In both NMF domains, four peaks separated by 90° were observed, meaning that two NMF phases with orthogonal b_O axes were present. For NMF(010) domains, the orthorhombic a_O and c_O axes ∥ STO [110]. For NMF(101) domains, the b_O axis commensurately aligns ∥ STO [010] and [$\bar{1}$00] (labeled D1 and D2 in Fig. 1d). For the NMF(010) domains, each $(222)_O$ reflection was additionally comprised of two peaks separated by 1.4° (Fig. 1b, inset). Therefore, each NMF(010) domain was actually comprised of two in-plane twin domains rotated by 1.4° about the surface normal with respect to each other (labeled D_3 and D_4 in Fig. 1b inset and 1d top view). Similar epitaxies of orthorhombically distorted perovskite oxide films on STO have been reported elsewhere.[24,26–28]

For the NMF/SRO sample, epitaxy could not be confirmed by ϕ-scans or RSM, despite the streaky RHEED pattern in Fig. 1a. This indicates that the bulk of NMF was highly disordered, with small domains. Because of the similarity between STO and SRO, however, it is reasonable to assume that the strain in the NMF/SRO sample was not too different from the NMF/STO sample.

The temperature-dependent magnetization measurements on NMF/STO were carried out by first cooling the samples from room temperature to 5 K in $H = 0$, and then measuring the magnetic moment m as a function of T in $H = 1$ kOe applied in-plane along the STO [001] direction while warming up to 320 K (zero-field cooled, ZFC). Then the measurements were continued while cooling in the same H down to 5 K (field cooled, FC). Subsequently, the thermoremanent magnetization (TRM) was measured while warming in $H = 0$. ZFC and FC data in Fig. 2a show a Curie-Weiss-like increase with decreasing temperature until the ZFC data peak at $T_N \approx 66$ K (see supplementary material). On the other hand, the FC m decreases sharply below $T_N \approx 66$ K, in good agreement with theory[21] and previous experimental work.[15–19] This split between ZFC and FC magnetizations below 66 K is consistent with weak FM below T_N, in agreement with previous studies of NMF nanoparticles and nanoplates.[19,20] The

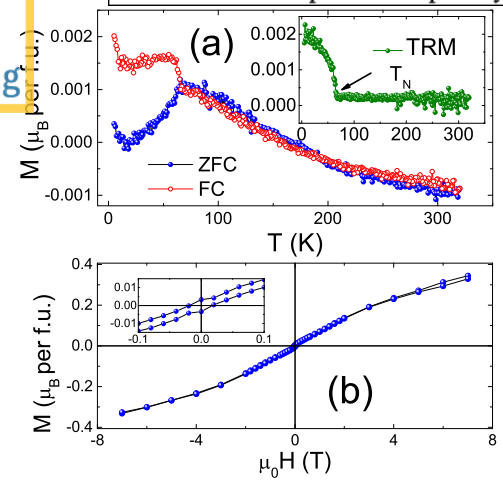

FIG. 2. Magnetic behavior of a 50 nm NMF/STO thin film. (a) FC and ZFC magnetic moment m as a function of temperature T. Inset shows TRM data. The negative FC and ZFC background is likely a result of an imperfect subtraction of the substrate signal. (b) In-plane magnetization M as a function of the applied magnetic field $\mu_0 H$ at 5 K. Inset shows close-up view of the low-field region.

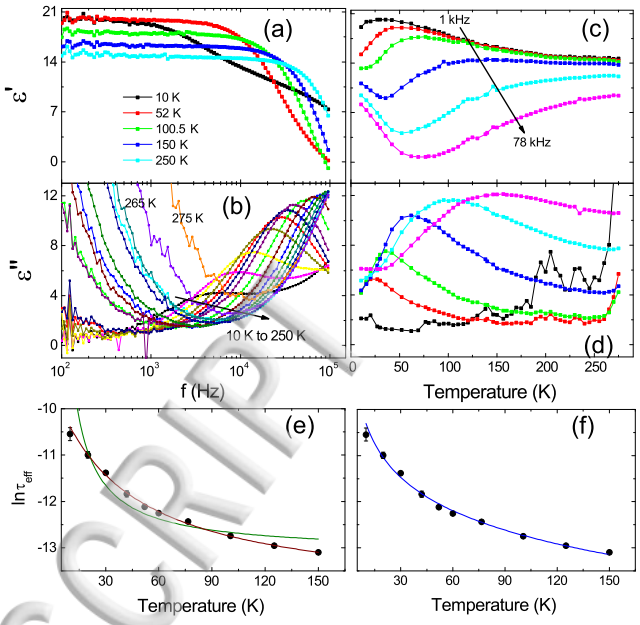

FIG. 3. Real (a) and imaginary (b) parts of the dielectric constant ε of the 150 nm NMF/SRO film as a function of frequency f at different temperatures T. Real (c) and imaginary (d) parts of $\varepsilon(T)$ at f = 1, 5, 10, 25, 50 and 78 kHz. Arrow in (c) points to the direction of increasing f. (e) Arrhenius law (olive curve), Vogel-Fulcher law (wine curve), and (f) power law (blue curve) fits of the temperature dependence of the relaxation time.

TRM data have a Brillouin-like increase below T_N, confirming the weak ferromagnetic nature of the transition. Fig 2b shows the in-plane magnetization hysteresis loop $M(H)$ measured at 5 K with the diamagnetic response from the substrate subtracted. The $M(H)$ behavior is consistent with weak FM, including an S-shaped loop with a lack of saturation in magnetic fields of up to 7 T and a remanent magnetization $M(H=0) \approx 0.003\ \mu_B$/f.u. in the low field region (Fig. 2b, inset).

Figure 3c and d shows the dielectric permittivity ε as a function of T for the 150 nm thick NMF/SRO film at frequencies from 1 to 78 kHz. The response at 0.1 kHz almost overlaps with that at 1 kHz so it is not shown. At large frequencies, the increase of the real part of the dielectric permittivity $\varepsilon'(T)$ at low T is superimposed with a broad maximum whose position shifts to lower T with decreasing frequency f. The imaginary part of dielectric permittivity, $\varepsilon''(T)$, also shows a peak that shifts to lower T and becomes narrower with decreasing f. This behavior implies a strong relaxation of the dielectric permittivity and resembles properties of relaxor ferroelectrics,[29] but the frequency dependence of the position of the maximum of $\varepsilon'(T)$, T_m, is much stronger than is typically observed in relaxors.[30] In our case, T_m shifts more than 200 K in only two frequency decades.

To gain more insight in relaxation dynamics, we analyzed f dependence of ε. At low f, $\varepsilon''(f)$ follows a $1/f$ dependence which is due to a non-zero dc conductivity (Fig. 3b). Also, a typical relaxation maximum is observed for $f > 3$ kHz, whose position shifts to lower f as T decreases. The $\varepsilon'(f)$ behavior shows a step-like increase at frequencies where $\varepsilon''(f)$ is a maximum. As T decreases below 52 K, another relaxation peak seems to appear at a higher frequency. However, this peak was not within our experimental window down to the lowest T, and only the low-f wing is visible.

Assuming a Debye-like dielectric relaxation, the broad peaks (steps) in the $\varepsilon''(f)$ ($\varepsilon'(f)$) data indicate the existence of a distribution of relaxation times. Using the Cole-Cole dispersion law,[31]

$$\varepsilon(f) = \varepsilon_\infty + \frac{\Delta\varepsilon}{1 + (i2\pi f \tau_{\text{eff}})^\beta}, \qquad (1)$$

where τ_{eff} is an effective characteristic relaxation time, ε_∞ is the dielectric permittivity at very high frequencies, $\Delta\varepsilon$ is the relaxation strength, and β ($0 < \beta \leq 1$) indicates the width of the relaxation time distribution ($\beta = 1$ corresponds to a Debye relaxation with a single relaxation time). The values of $\tau_{\text{eff}}(T)$, extracted from the position of the maximum of $\varepsilon''(f)$, $\tau_{\text{eff}} = (2\pi f_m)^{-1}$, are shown in Figs. 3e-f. $\tau_{\text{eff}}(T)$ cannot be fitted well either by an Arrhenius law,

$$\tau_{\text{eff}}(T) = \tau_0 \exp(-E_a/kT), \qquad (2)$$

or by a Vogel-Fulcher law applicable to typical relaxor FE,

$$\tau_{\text{eff}}(T) = \tau_0 \exp[-E_a/k(T - T_f)], \qquad (3)$$

where k is Boltzmann's constant and E_a is an activation energy, as seen in Fig. 3e. In the case of Eq. 2, the quality of the fit is low, while the fit to Eq. 3 results in an unphysical negative value of the freezing temperature, T_f. On the other hand, $\tau_{\text{eff}}(T)$ is described well by the power law equation

$$\tau_{\text{eff}}(T) = \tau_0 (T/T_0 - 1)^\nu. \qquad (4)$$

The best fit (Fig. 3f) yields $\nu = -0.90 \pm 0.07$, $\tau_0 = (2.8 \pm 1.5) \times 10^{-5}$ s, and a transition temperature $T_0 = 8$ K. The value of ν is close to $\nu = -1$ that describes the divergence of the relaxation time for an order-disorder phase transition in the classical mean-field approximation.[32] The actual transition temperature could be much lower than 8 K because only the behavior for $T > T_0$ was observed. Interestingly, in canonical ferroelectrics the relaxation dynamics corresponding to such transition are typically observed in the GHz frequency range, indicating that relaxing dipolar entities are relatively large and slowly fluctuating microscopic regions spanning several unit cells.

Large dielectric dipolar regions could form because of the diffusion of a FE soft mode[21,22] as a result of the disorder in the NMF/SRO film. Although the NMF/STO film has only a small strain, local measurements like piezoelectric force microscopy (PFM) need to be performed to verify ferroelectricity because of the lack of an electrically conductive bottom layer. In addition, further research is required to obtain a tetragonal $a_O = c_O$ lattice distortion in $NaMnF_3$ thin films to verify the large ferroelectric polarization predicted by theory.[21,22]

See supplementary material for details of the growth procedure and structural characteristics of the films, as well as magnetic susceptibility data.

This work was supported by the National Science Foundation (grant # 1434897) and the WVU Shared Research Facilities. We thank A. H. Romero and C. Chen for helpful discussions.

[1] W. Eerenstein, N. Mathur, and J. F. Scott, Nature **442**, 759 (2006).
[2] M. Fiebig, Journal of Physics D: Applied Physics **38**, R123 (2005).
[3] S. Cherepov, P. Khalili Amiri, J. G. Alzate, K. Wong, M. Lewis, P. Upadhyaya, J. Nath, M. Bao, A. Bur, T. Wu, G. P. Carman, A. Khitun, and K. L. Wang, Applied Physics Letters **104**, 082403 (2014).
[4] S.-W. Cheong and M. Mostovoy, Nature materials **6**, 13 (2007).
[5] P. Hayes, S. Salzer, J. Reermann, E. Yarar, V. Rbisch, A. Piorra, D. Meyners, M. Hft, R. Knchel, G. Schmidt, and E. Quandt, Applied Physics Letters **108**, 182902 (2016).
[6] T. Zhao, A. Scholl, F. Zavaliche, K. Lee, M. Barry, A. Doran, M. Cruz, Y. Chu, C. Ederer, N. Spaldin, et al., Nature materials **5**, 823 (2006).
[7] T.-J. Park, G. C. Papaefthymiou, A. J. Viescas, A. R. Moodenbaugh, and S. S. Wong, Nano Letters **7**, 766 (2007).
[8] W.-G. Yang, N. A. Morley, J. Sharp, Y. Tian, and W. M. Rainforth, Applied Physics Letters **108**, 012901 (2016).
[9] J. S. Hwang, J. Y. Cho, S. Y. Park, Y. J. Yoo, P. S. Yoo, B. W. Lee, and Y. P. Lee, Applied Physics Letters **106**, 062902 (2015).
[10] J. F. Scott and R. Blinc, Journal of Physics: Condensed Matter **23**, 113202 (2011).
[11] R. E. Cohen, Nature **358**, 136 (1992).
[12] J. Ravez, Comptes Rendus de l'Académie des Sciences - Series {IIC} - Chemistry **3**, 267 (2000).
[13] P. Borisov, T. A. Johnson, A. C. Garca-Castro, A. KC, D. Schrecongost, C. Cen, A. H. Romero, and D. Lederman, ACS Applied Materials & Interfaces **8**, 2694 (2016).
[14] A. Ratuszna, K. Majewska, and T. Lis, Acta Crystallographica Section C **45**, 548 (1989).
[15] S. Pickart, H. Alperin, and R. Nathans, Journal de Physique **25**, 565 (1964).
[16] J. R. Shane, D. H. Lyons, and M. Kestigian, Journal of Applied Physics **38**, 1280 (1967).
[17] D. Teaney, J. Blackburn, and R. Stevenson, Bull. Am. Phys. Soc. **7**, 201 (1962).
[18] P. Daniel, M. Rousseau, A. Desert, A. Ratuszna, and F. Ganot, Phys. Rev. B **51**, 12337 (1995).
[19] E. E. Carpenter, C. Sangregorio, and C. J. O'connor, Mol. Cryst. Liq. Crys. A **334**, 641 (1999).
[20] Y.-P. Du, Y.-W. Zhang, Z.-G. Yan, L.-D. Sun, S. Gao, and C.-H. Yan, Chemistry An Asian Journal **2**, 965 (2007).
[21] A. C. Garcia-Castro, N. A. Spaldin, A. H. Romero, and E. Bousquet, Phys. Rev. B **89**, 104107 (2014).
[22] A. C. Garcia-Castro, A. H. Romero, and E. Bousquet, Phys. Rev. Lett. **116**, 117202 (2016).
[23] J. G. Connell, B. J. Isaac, G. B. Ekanayake, D. R. Strachan, and S. S. A. Seo, Applied Physics Letters **101**, 251607 (2012).
[24] S. S. Kim, T. S. Kang, and J. H. Je, Journal of Applied Physics **90**, 4407 (2001).
[25] M. Björck and G. Andersson, Journal of Applied Crystallography **40**, 1174 (2007).
[26] X. Martí, F. Sánchez, V. Skumryev, V. Laukhin, C. Ferrater, M. García-Cuenca, M. Varela, and J. Fontcuberta, Thin Solid Films **516**, 4899 (2008).
[27] C. J. M. Daumont, D. Mannix, S. Venkatesan, G. Catalan, D. Rubi, B. J. Kooi, J. T. M. D. Hosson, and B. Noheda, Journal of Physics: Condensed Matter **21**, 182001 (2009).
[28] J. Scola, P. Boullay, W. Noun, E. Popova, Y. Dumont, A. Fouchet, and N. Keller, Journal of Applied Physics **110**, 043928 (2011).
[29] A. Bokov and Z.-G. Ye, in Frontiers of Ferroelectricity (Springer, 2006) pp. 31–52.
[30] G. A. Samara, Journal of Physics: Condensed Matter **15**, R367 (2003).
[31] F. Kremer and A. Schönhals, eds., Broadband Dielectric Spectroscopy (Springer, Berlin, Heidelberg, 2003).
[32] M. E. Lines and A. M. Glass, Principles and applications of ferroelectrics and related materials (Claredon Press, Oxford, 2004).

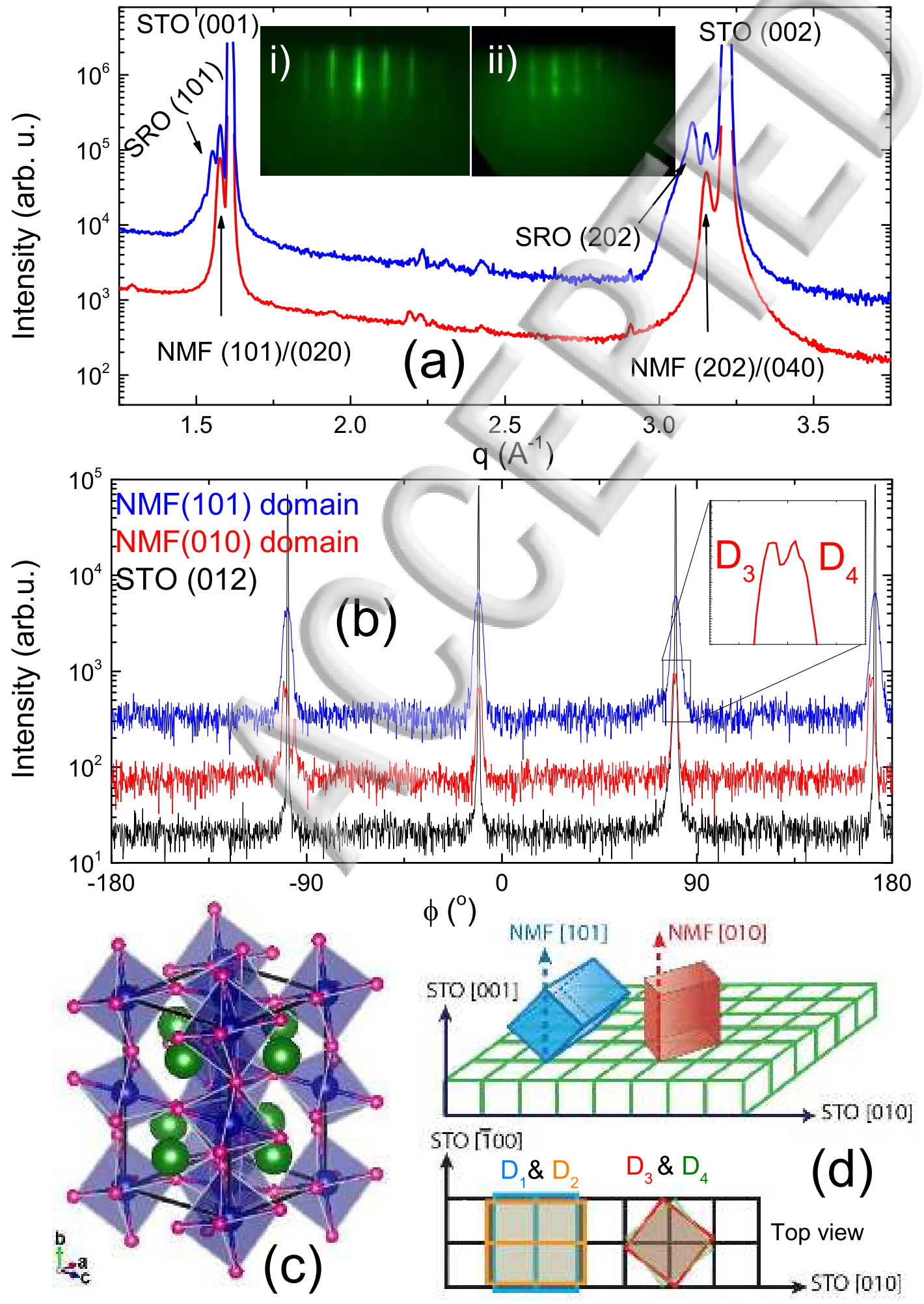
STO (001)
SRO (101)
i)
ii)
STO (002)
SRO (202)
NMF (101)/(020)
NMF (202)/(040)
(a)
Intensity (arb. u.)
q (A^{-1})
NMF(101) domain
NMF(010) domain
STO (012)
(b)
D$_3$
D$_4$
ϕ (°)
(c)
NMF [101]
NMF [010]
STO [001]
STO [010]
STO [$\bar{1}$00]
D$_1$& D$_2$
D$_3$ & D$_4$
(d)
Top view
STO [010]

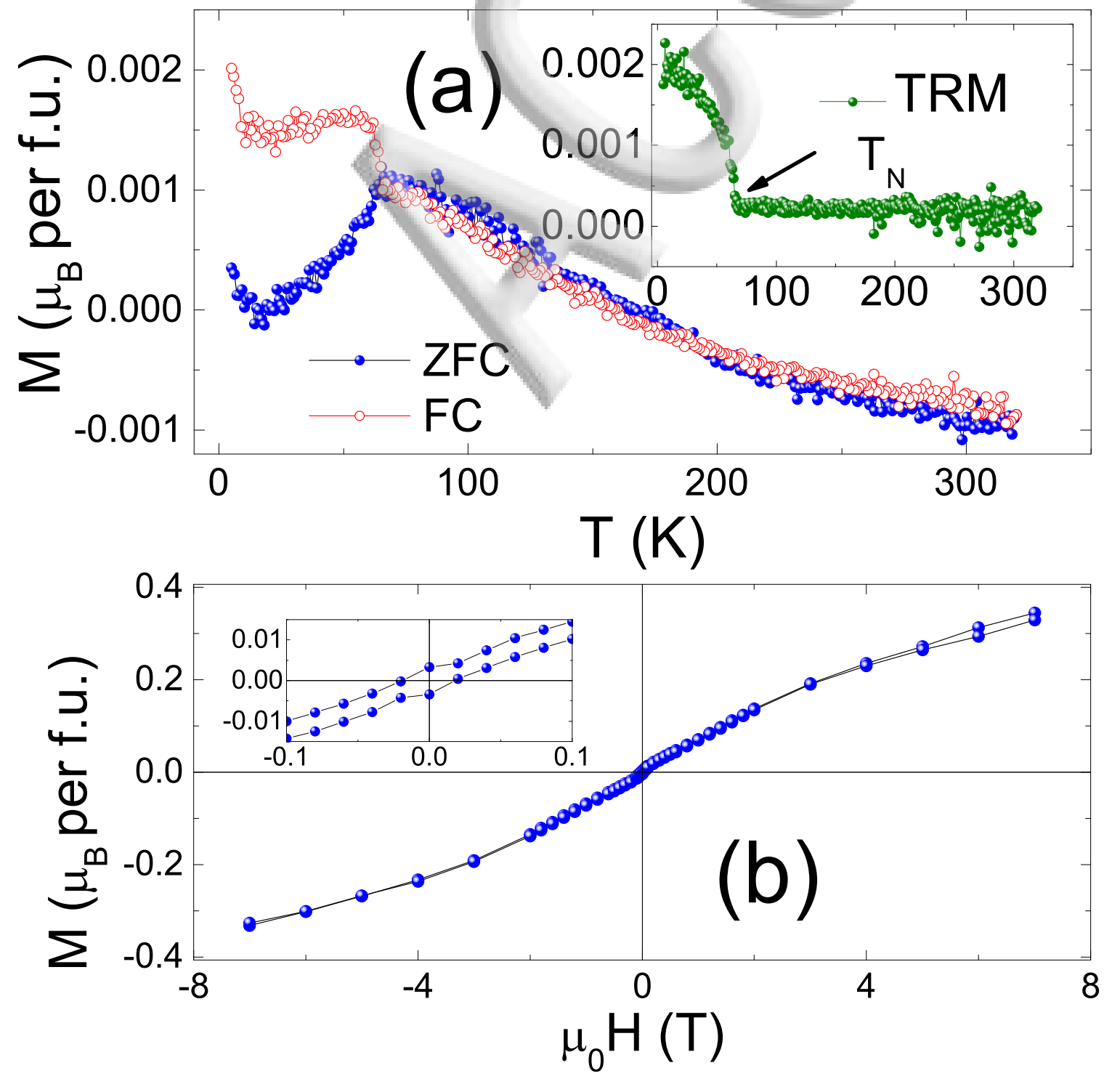
(a)
M (μB per f.u.)
0.002
0.001
0.000
-0.001
0
100
200
300
T (K)
ZFC
FC
TRM
TN
0.002
0.001
0.000
0
100
200
300
(b)
M (μB per f.u.)
0.4
0.2
0.0
-0.2
-0.4
-8
-4
0
4
8
μ0H (T)
0.01
0.00
-0.01
-0.1
0.0
0.1

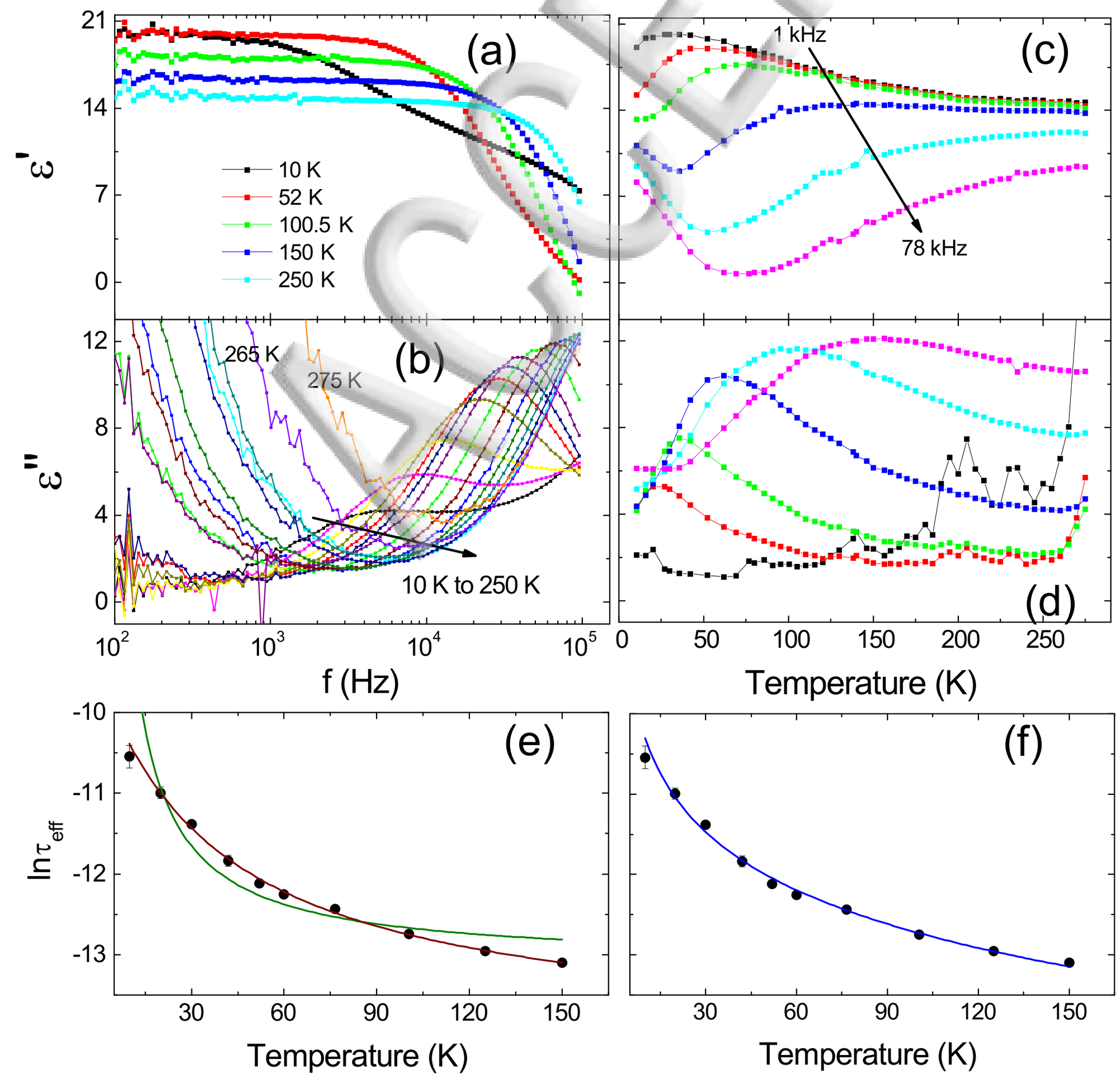
(a)
(b)
(c)
(d)
(e)
(f)
ε'
ε''
10 K
52 K
100.5 K
150 K
250 K
265 K
275 K
10 K to 250 K
1 kHz
78 kHz
f (Hz)
Temperature (K)
Temperature (K)
ln τeff